5-13-2020

Kidney Tomosynthesis Image Reconstruction Algorithms and Image Quality Evaluation

Allison McMinn
Southern Illinois University Carbondale, allison.mcminn@siu.edu

Ying Chen
Southern Illinois University Carbondale, adachen@siu.edu

Kidney Tomosynthesis Image Reconstruction Algorithms and Image Quality Evaluation

Allison McMinn

A thesis submitted to the University Honors Program
in partial fulfillment of the requirements for the
Honors Certificate with Thesis

Approved By:
Dr. Ying Chen

Southern Illinois University Carbondale
Date: 13 May 2020

Kidney Tomosynthesis Image Reconstruction Algorithms and Image Quality Evaluation

Allison McMinn*, Ying Chen*

*Department of Electrical and Computer Engineering, Southern Illinois University Carbondale, IL 62901 USA

Abstract: Kidney stone disease is one of the most common diseases that faces the American population. For proper diagnosis of kidney stones medical imaging must be performed. The current gold standard for kidney stone detection is computed tomography (CT) imaging. However, CT imaging exposes the patient to large amounts of x-ray radiation. Digital tomosynthesis is a novel technique in medical diagnosis due to its ability to generate high-resolution images while limiting the radiation dosage to patients in comparison to CT imaging. Tomosynthesis is a three-dimensional imaging technique that allows the reconstruction of an arbitrary set of planes from limited-angle series of projection images. Tomosynthesis has well-published success in the field of breast and chest imaging but has had limited studies performed in field of kidney imaging. In this study, C-arm geometry tomosynthesis was compared to traditional tomosynthesis using the shift and add reconstruction algorithm to evaluate the effectiveness of C-arm tomosynthesis in the application of kidney imaging. A simulation was created to generate projection images of each geometry and implement the shift and add algorithm. The results showed that image reconstruction was possible using C-arm tomosynthesis geometry. However, it was observed that there was more blurring using C-arm tomosynthesis as compared to traditional tomosynthesis which can likely be attributed to the increased isocentric motion in the C-arm geometry. This indicates that C-arm tomosynthesis geometry has the potential to be developed with other reconstruction algorithms to make it better suited for implementation in kidney imaging. Furthermore, the simulations developed in this study lay the groundwork for future development of C-arm tomosynthesis by providing a platform to test new reconstruction algorithms and optimize system parameters for clinical applications.

I. Introduction

A. Clinical Motivations

In the United States, kidney stone disease affects up to 12% of the American population. This makes kidney stone disease one of the most common diseases in America. Kidney stone disease presents symptoms similar to many other abdominal conditions which makes imaging an essential tool required to confirm a kidney stone diagnosis [1]. Oftentimes multiple rounds of imaging are required to track the movement of the stone to ensure that therapies are working and to make sure there are no complications.

Various imaging techniques are available to diagnose patients with symptoms of renal or urinary tract disease, including plain renal ultrasonography, and computed tomography (CT) [2,3]. Ultrasound imaging does not have

the capability to produce high resolution images and is usually only used as a secondary diagnostic confirmation [1]. The low image quality in ultrasound imaging can be a detriment when trying to implement new therapies such as Extracorporeal shock wave lithotripsy, ESWL [4]. In this procedure the exact location of the stone must be known so that the shock waves can be aimed properly to break-up the stone.

Currently, computed tomography (CT) is the gold standard of imaging for detecting kidney stones disease [1]. CT imaging produces high-resolution images that can accurately locate stones in the urinary track. One of the major drawbacks of CT imaging is that it exposes the patient to large amounts of x-ray radiation. The expanded use of CT imaging is likely related to the increase of average radiation dosage experienced by individuals in a year [5]. The drawn-out procedure time can also have impacts to the total cost incurred by the patient.

B. Traditional Tomosynthesis

Tomosynthesis is a three-dimensional imaging technique that allows for the reconstruction of an arbitrary set of planes from a limited-angle series of projection images. Digital tomosynthesis is a novel technique in medical diagnosis due to its ability to create high resolution images compared to standard two-dimensional techniques and reduced radiation dosages compared to CT imaging. [2]. Improving this technology has the potential to increase patient health by detecting conditions earlier and with higher accuracy. It also has the potential to reduce medical expenses by reducing procedure time as compared to CT. Figure 1 shows a traditional breast tomosynthesis geometry that is used in

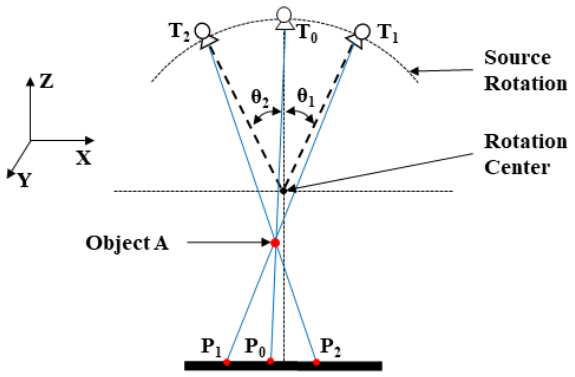

Figure 1: Traditional tomosynthesis geometry diagram. T represents the X-ray source location and P represents where point A will appear on the detector plane. θ is the rotation angle of the X-ray source.

tomosynthesis imaging. The key characteristic of traditional tomosynthesis is that the X-ray source rotates but the detector plate remains stationary. Tomosynthesis has well-published success in the field of breast and chest imaging but has had limited studies performed in kidney imaging [3].

A handful of studies have been conducted to assess the feasibility of utilizing tomosynthesis in kidney imaging. A study by Liu on live patients compared to traditional Kidneys-Ureters-Bladder radiograph (KBU), unenhanced multidetector computed tomography (UMDCT), and digital tomosynthesis in the detection of kidney stones, and concluded that digital tomosynthesis provided more precise results than KUB radiography without the high dosage levels of UMDCT [6]. Other studies by the academic community showed that utilizing deblurring algorithms such as filtered back projection reconstruction algorithm showed superior results to traditional image reconstruction algorithms in breast tomosynthesis imaging [7]. These new advancements of digital tomosynthesis can be applied to kidney imaging to improve kidney stone detection and tracking.

C. C-arm Tomosynthesis

A C-arm is a medical imaging machine that has been in use since the 1950s. It gets its name from the C shaped arm that holds the x-ray source and detector [8]. These devices are traditionally used in operating rooms to provide real time images at any location on a patient's body [9]. The major difference in this method of imaging is that the detector plate moves with the X-ray source as demonstrated in Figure 2. C-arm machines can be used to image the abdominal area of a patient unlike tradition tomosynthesis machines. For this reason, a C-arm geometry was investigated for the use in kidney tomosynthesis.

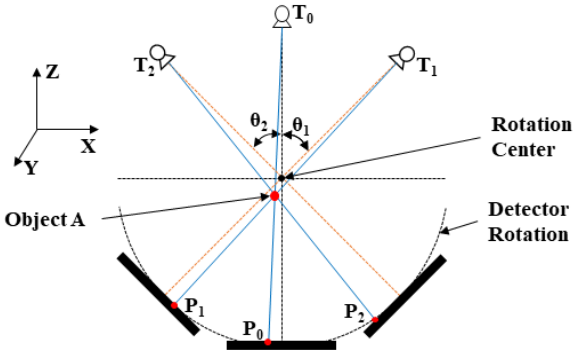

Figure 2: C-arm tomosynthesis geometry diagram. T represents the X-ray source location and P represents where point A will appear on the detector plane. θ is the rotation angle of the X-ray source and detector plate.

D. Shift and Add Reconstruction Algorithm

As discussed previously, there are many reconstruction algorithms that have been successfully implemented in traditional tomosynthesis. Shift and Add is one of the staple 3D image reconstruction algorithms and is the basis upon which many other algorithms have been developed [10]. In principle, the algorithm shifts each projection image in the x-direction a specific amount based on the source angle and the reconstruction plane height. The pixel values of each of the shifted projection images are then added and the average of their values is taken. Figure 3 demonstrates the shifting of the projection's images and the need to zero-pad the reconstruction image size so that one does not lose any information in the process of reconstructing.

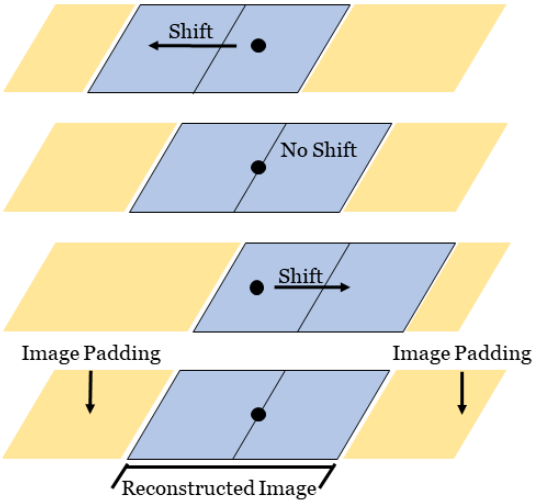

Figure 3: Diagram depicting the shift and add reconstruction method that requires zero-padding on the reconstruction image. The arrows represent the direction that projection images were shifted.

For traditional tomosynthesis the shift amount is given by equation 1 below:

$$Shift(z) = L \sin\theta \frac{Z}{L\cos\theta + (SID - L - Z)} \quad (1)$$

Where L is the arm length of the source, SID is the source to image distance, Z is the height of the reconstruction plane, and θ is the arm rotation angle for the given projection image.

For C-arm tomosynthesis simulated geometry in this study, the shift amount can be simplified to equation 2 below.

$$Shift(z) = Z \tan\theta \quad (2)$$

Where Z is the height of the reconstruction plane, and θ is the arm rotation angle for the given projection image. Shift and Add

reconstruction was selected for this study due to its simplicity in implementation with a new geometry.

II. Methods

A. Geometry Derivations:

To perform this study a set of simulated projection images needed to be created. This required deriving equations that would calculate the location that a simulated object would appear on the detector plane at a given orientation of the x-ray source. The equations for traditional tomosynthesis were derived in given below.

$$P_{xi} = T_{xi} - T_{zi}\frac{(T_{xi}-A_x)}{(T_{zi}-A_z)} \quad (1)$$

$$P_{yi} = T_{yi} - T_{zi}\frac{(T_{yi}-A_y)}{(T_{zi}-A_z)} \quad (2)$$

Where $P_i(X,Y)$ represents the position of projected point on the detector plane at a given rotation of the source arm, $T_i(X,Y,Z)$ represents the source position at a given rotation of the source arm, and A(X,Y,Z) is the position of an object being projected.

Due to the differences in the geometry between traditional and C-arm tomosynthesis, a new set of equations need to be derived for C-arm geometry. In principle, the projected image location can be calculated using the same procedure as traditional tomosynthesis. However, the X-Z plane is rotating with the x-ray source and detector. So, a new coordinate system can be defined dependent on the arm rotation. By converting each of the points into this new coordinate system the projection images can be generated. The equations are given below.

$$A_u = A_x\cos\theta - A_z\sin\theta \quad (3)$$

$$A_z = A_z\cos\theta - A_x\sin\theta \quad (4)$$

$$T_{ui} = T_{xi} \quad (5)$$

$$T_{vi} = T_{zi} \quad (6)$$

$$P_{ui} = T_{ui} - T_{vi}\frac{(T_{ui}-A_u)}{(T_{vi}-A_v)} \quad (7)$$

$$P_{yi} = T_{yi} - T_{vi}\frac{(T_{yi}-A_y)}{(T_{vi}-A_v)} \quad (8)$$

Where $P_i(U,Y,V)$ represents the position of projected point on the detector plane at a given rotation (θ) of the source arm, $T_i(X,Y,Z)$ represents the source position at a given rotation (θ) of the source arm and A(X,Y,Z) is the position of an object being projected.

B. Computer Simulation

To evaluate the effectiveness of C-arm geometry tomosynthesis a computer simulation was developed. This program simulates the projection images for both traditional and C-arm tomosynthesis imaging. The shift and add reconstruction algorithm were then applied to each and the results were compared. The coding logic flow diagram for this simulation is provided in Figure 4.

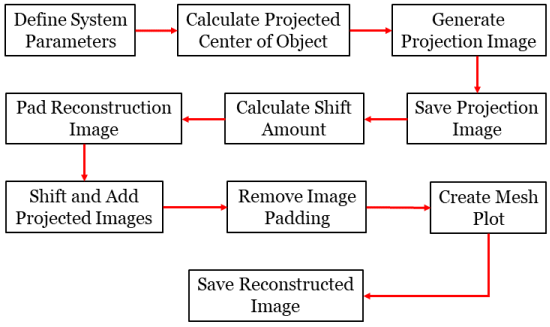

Figure 4: Simulation coding logic flow diagram.

The following parameters where used in generating the computer simulated projections images, for this preliminary study. Some of the imaging parameters, such as number of projection images, can be

adjusted with flexibility and leave room for optimization in future studies.

Source to Image Distance = 180 cm
Source Arm Length = 150 cm
Air Gap = 8 cm
Angle swept = +/- 30 degrees
Image Size = 1024 X 1024 Pixels
Number of Projection Images = 41
Number of Reconstruction Planes = 41
Pixel Size = 0.02 cm
Object Center Location = (0 cm,-4 cm,10 cm)
Object Radius = 0.2 cm
Object Height = 4 cm

III. Results

A. Projection Image Generation

Projection images were successfully generated for both traditional and C-arm tomosynthesis imaging. Figure 5 A-F show projection images for each geometry at -15 degrees, 0 degrees, and 15 degrees of arm rotation. It can be observed that the projection is traveling across the detector as the x-ray source arm moves. The middle projection images show that the object appears at the same location for each geometry as one would expect.

B. Shift and Add Reconstruction

The simulated projection images were able to be successfully reconstructed using the shift and add reconstruction algorithm. Figure 6 and 7 show the reconstructed images for traditional and C-arm tomosynthesis geometries at a reconstruction height of 10 cm respectively. This is the reconstruction height where the object is located. In an ideal reconstruction these images would be a replica of the middle projection (Theta = 0 degrees) images from Figure 5. One can observe that in both images there is a small amount of blurring that occurs around the response. However, the c-arm geometry in Figure 7 exhibits a larger amount of blurring

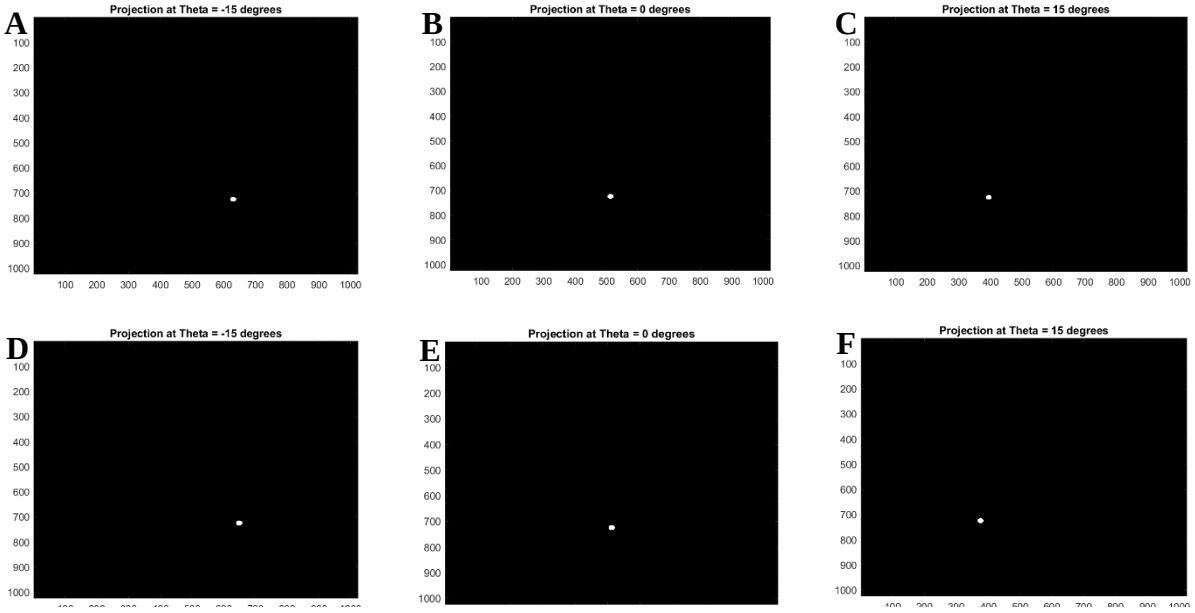

Figure 5: A-C: Projection images using traditional tomosynthesis geometry at a x-ray source angle of -15, 0, 15 degrees respectively. D-F: Projection images using C-arm tomosynthesis geometry at a x-ray source angle of -15, 0, 15 degrees respectively.

around the response than that of the traditional tomosynthesis in Figure 6.

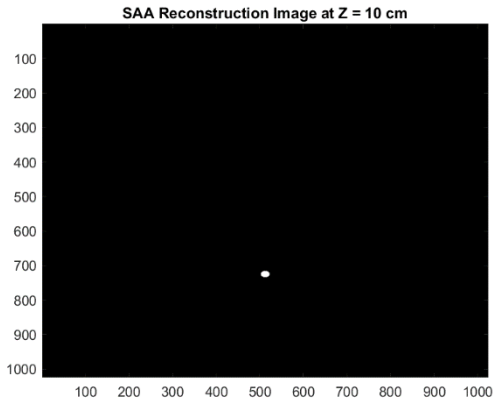

Figure 6: Reconstructed image at Z = 10 cm using traditional tomosynthesis and SAA reconstruction algorithm.

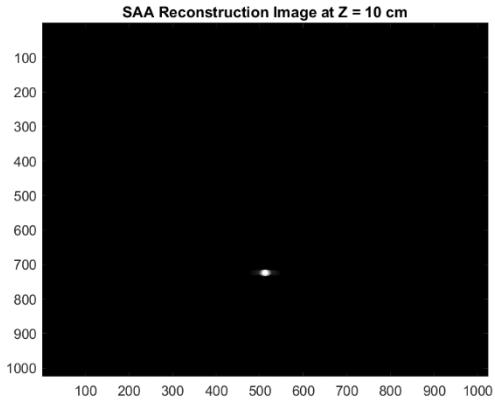

Figure 7: Reconstructed image at Z = 10 cm using C-arm tomosynthesis and SAA reconstruction algorithm.

Mesh plots were created to evaluate the pixel values at each location. Figure 8 and 9 show the mesh plots for both traditional and C-arm tomosynthesis geometries at a reconstruction height of 10 cm respectively. Normalizations can be performed to further compare the responses in reconstructed images, based on in-plane sharpness and out-of-plane blurring evaluations.

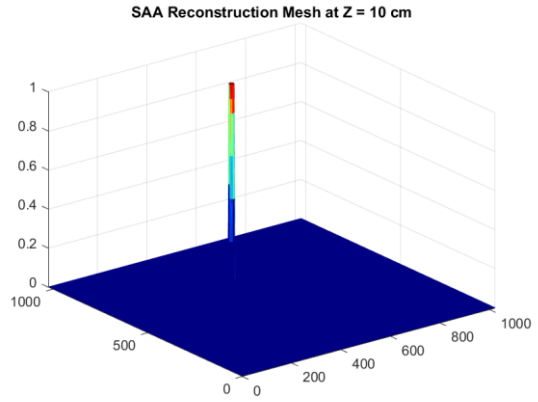

Figure 8: Mesh Plot of the reconstructed image at Z = 10 cm using traditional tomosynthesis and SAA reconstruction algorithm.

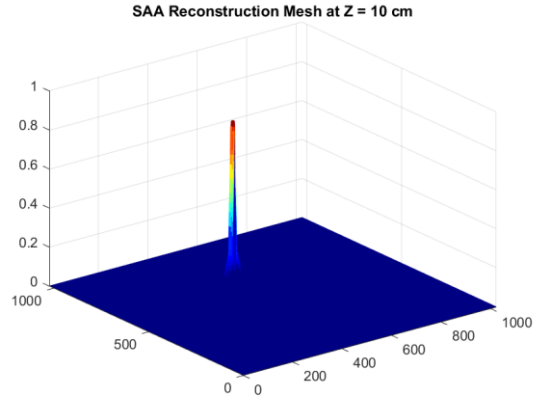

Figure 9: Mesh Plot of the reconstructed image at Z = 10 cm using C-arm tomosynthesis and SAA reconstruction algorithm.

C. Artifact Blurring

One of the key characteristics of shift and add reconstruction is that artifacts are only in focus when the reconstruction plane height is equal to the artifact height. To demonstrate that this occurs with each tomosynthesis geometry an additional study was conducted. In this study a second object was added at a height of 11 cm. Figure 10 A-D show the reconstructed images for both traditional and C-arm tomosynthesis geometries at a reconstruction height of 10 cm and 11 cm.

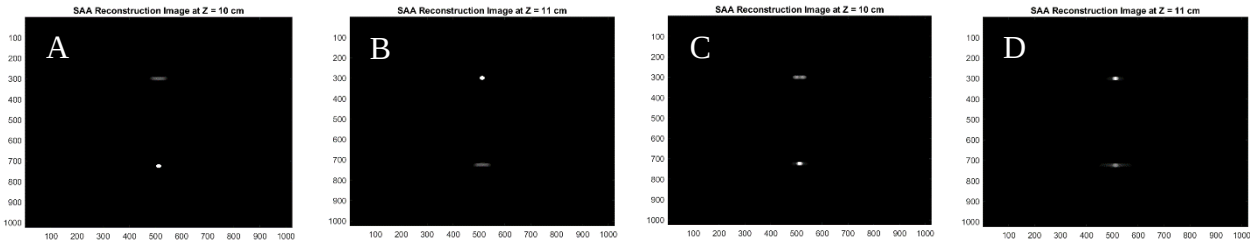

Figure 10: A-B: Reconstructed image using traditional tomosynthesis geometry at a reconstruction plane height of Z = 10 cm and Z = 11 cm respectively. C-D: Reconstructed image using C-arm tomosynthesis geometry at a reconstruction plane height of Z = 10 cm and Z = 11 cm respectively.

The images show that for each geometry one object is in focus and the other is blurred in a line at 10 cm. It can then be observed that at 11 cm the objects switch which one is in focus and which one is blurred.

IV. Discussion

The results of this study demonstrated the successful generation of projection images for both traditional and C-arm tomosynthesis geometries. These projection images were then passed through a shift and add reconstruction algorithm. Initial observations indicated that the C-arm geometry had more blurring around the edges of the response. When an analysis of the mesh plots of the pixel values was conducted this observation was supported. The extra blurring around the object and lower pixel values is likely due to the increased isocentric motion of the C-arm. When analyzing the reconstructed images with two objects observations showed similar artifact blurring between the two tomosynthesis geometries. For both geometries it was observed that the reconstructed objects came into focus at their corresponding correct heights. Further development of c-arm tomosynthesis methods can be pursed to improve kidney imaging techniques.

V. Conclusion

This work has demonstrated that the C-arm geometry tomosynthesis required for kidney imaging produces comparable results to that of traditional tomosynthesis when using a shift and add reconstruction algorithm. This means that future works can be performed to develop other reconstruction algorithms for C-arm geometry tomosynthesis. Furthermore, additional studies can be performed to optimize parameters of this simulation, such as number of projections and reconstruction plane spacing. Further development of C-arm geometry tomosynthesis may benefit future advancements for kidney imaging and kidney stone detection methods and therapies.

VI. Acknowledgments

I would like to thank Dr. Ying Chen for serving as my faculty advisor for this project and for serving as my research mentor over the past three years at SIU. I would also like to thank the McNair Scholars Program for their continued support of all my research activities. Finally, I would like to thank the University Honors Program for supporting this project as an honors thesis and their mentorship over my entire four years at SIU.

VII. About the Author

Allison McMinn is a senior majoring in Electrical Engineering at Southern Illinois University Carbondale. She has been a member of the University Honors program for all four years. She is also proud to be a member of the Ronald E. McNair Scholars Program at SIU. Allison has been conducting research at SIU for the past four years. Allison received a National Science Foundation Graduate Research Fellowship and a Dean's Fellowship to fund her continued education at Arizona State University. Allison will be pursuing a Ph.D. in Electrical Engineering with the intention of becoming a professor.

VIII. References

[1] M. Schubbe, E. Tackacs, "Medical Student Curriculum: Kidney Stones" American Urological Association, Web, 2019.

[2] N. A. Malalla, P. Sun, Y. Chen, M. Lipkin, G. M. Preminger, and J. Qin, "C-arm technique with distance driven for nephrolithiasis and kidney stones detection: preliminary study", Proceeding of 2016 IEEE-EMBS International Conference on Biomedical and Health Infomratics (BHI), 2016, pp. 164-167.

[3] J. Qin, W.N. Simmons, G. Sankin, P. Zhong, "Effect of lithotripter focal width on stone comminution in shock wave lithotripsy." The Journal of the Acoustical Society of America, vol 127(4), 2010, pp. 2635-2645.

[4] "Extracorporeal Shock Wave Lithotripsy (ESWL) for Kidney Stones", Michigan Medicine, University of Michigan, Web, 11 August 2019.

[5] A. Neisius, G. Astroza, C. Wang, G. Nguyen, N. Kuntz, N. Januzis, M. Ferrandino, T. Yoshizumi, G. Preminger, M. Lipkin, "Digital Tomosynthesis: A New Technique for Imaging Nephrolithiasis. Specific Organ Doses and Effective Doses Compared With Renal Stone Protocol Noncontrast Computed Tomography" Urology, Vol 83, pp 282-287.

[6] S. Liu, H. Wang, W. Feng, X. Hu, J. Guo, Q. Shang, Z. Li, H. Yu, "The value of X-ray digital tomosynthesis in the diagnosis of urinary calculi", Experimental and Therapeutic Medicine 15, 2018, pp. 1749-1753.

[7] Y. Chen, J. Lo, J. Dobbins, "Impulse response and Modulation Transfer Function analysis for Shift-And-Add and Back Projection image reconstruction algorithms in Digital Breast Tomosynthesis (DBT)", Int. J. Functional Informatics and Personalised Medicine, Vol. 1, No. 2, pp.189–204.

[8] "What is a Mobile C-arm", Ziehm Imaging. Web. 2020.

[9] D. Fornell. "An Introduction to Mobile C-Arm X-Ray Systems", Imaging Technology News, Web, 13 April 2011.

[10] Y. Chen, J. Lo, J, Dobbins, "Importance of point-by-point back projection correction for isocentric motion in digital breast tomosynthesis: Relevance to morphology of structures such as microcalcifications – need to site still", Medical Physics, Vol 34, No. 10.

[11] S. Xu, J. Lu, O. Zhou, Y. Chen, "Statistical iterative reconstruction to improve image quality for digital breast tomosynthesis", Medical Physics, Vol. 42, No. 9.

[12] N. Malalla, P. Sun, Y. Chen, M. Lipkin, G. Preminger, J. Qin. "Preliminary Study on C-arm Technique for Nephrolithiasis and Kidney Stones Detection", IEEE International Conference on Bioinforrnatics and Biomedicine, 2015.

[13] N. Malalla, S. Xu, Y. Chen. “Limited Angle C-arm Tomosynthesis Reconstruction Algorithms”, International Society for Optics and Photonics, 2015.
[14] I. Wells, V. Raju, B. Rowberry. S. Johns, S. Freeman, “Digital tomosynthesis—a new lease of life for the intravenousurogram?”, The British Journal of Radiology, Vol. 84, pp. 464-468.
[15] T. Wu, A. Stewart, M. Stanton, T. McCauley, W. Phillips, D. Kopans, R. Moore, J. Eberhand, B. Opsahl-Ong, L. Niklason, M. Williams, “Tomographic mammography using a limited number of low-dose conebeam projection images”, Medical Physics, Vol. 30, No. 3.